Electronic Supplementary Material (ESI) for Nanoscale.

Supporting Information

Effects of graphene oxide nanosheets on ultrastructure and biophysical properties of pulmonary surfactant film

Qinglin Hu, Bao Jiao, Xinghua Shi, Russell P. Valle, Yi Y. Zuo,* and Guoqing Hu*

Simulation methods and results

Establishment of the CGMD models. In our CGMD simulations, the MARTINI force field[1] was used. The simulation parameters of CG DPPC, CG POPG and CG cholesterol were taken from the Martini force field. CG models of mini-B and SP-C were derived by analyzing their all-atom models obtained from the protein data bank. Four types of GO nanosheets were considered: 5×5 nm^2 monolayer, 5×5 nm^2 trilayer, 10×10 nm^2 monolayer, and 10×10 nm^2 trilayer. According to the widely accepted structure of GO by Lerf and Klinowski,[2] most of oxygen functional groups on the graphene basal plane are epoxy and hydroxyl groups. Thus we only considered these two types of groups in our model. The CG bead types SN0 and SP2 were used for constructing the C−O−C and C−OH groups respectively.[3] We adopted a neutral GO model in which the acidity of hydroxyl combining with benzene carbon atoms is considered negligible, although the hydroxyl groups in GO ionize and make itself anionic.[4,5]

The PS monolayer in our simulation consists of dipalmitoyl DPPC and POPG with a 7:3 molar ratio, doped with 10 wt % cholesterol, 1.6 wt % SP-B, and 1.5 wt % SP-C. Although the phospholipid system is simpler than natural PS, it contains both zwitterionic (PC) and anionic (PG) lipid headgroups, and both disaturated (dipalmitoyl) and unsaturated (palmitoyl-oleoyl) acyl chains. The SP-A and SP-D proteins are ignored as they are weakly associated with the PS film and have little to do with the biophysical function of the PS. Similar model systems have been proven to simulate biophysical properties of the natural PS *in vitro*[6] and *in silico*.[7,8] CG models for SP-B and SP-C were derived from their all-atom models in the protein data bank. The SP-C model (PDB ID: 1SPF) has two palmitoyl tails which is critical for its chemical properties.[9] We further improved our previous model[7] by adding cholesterols to represent neutral lipids and using mini-B, a more realistic model of SP-B, instead of SP-B_{1-25}. All simulations were performed using the GROMACS 4.5.4.[10]

Advantage of using mini-B instead of SP-B_{1-25}. The full-length human surfactant protein B (SP-B) contains 79 amino acid residues. SP-B_{1-25} (PDB: 1DFW) is a 25-residue peptide based on the N-terminal domain of full-length SP-B[11] whereas mini-B (PDB: 2DWF) is a 34-residue peptide which is composed of the N- and C-terminal helical regions of full-length SP-B.[12] Although detailed structure of the full-length SP-B has not been obtained, mini-B has been shown to retain similar activity to full-length SP-B to certain extent.[12,13] Schematics of SP-B_{1-25} and mini-B are show in Figure S1.

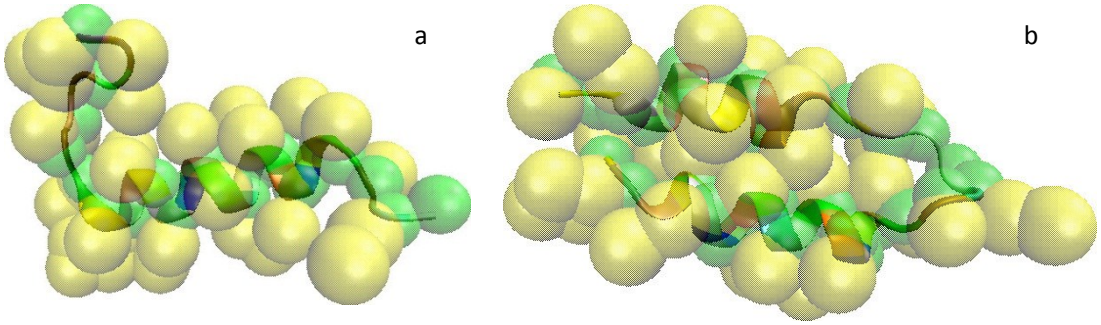

Figure S1. Schematics of SP-B_{1-25} (a) and mini-B (b). Bands denote the peptide structures, while spheres denote the beads in CG models.

Obtaining a stable PS monolayer interface. The equilibrium of the membrane was not established in one step. Firstly, a small system containing 70 CG DPPC, 30 CG POPG, 25 CG cholesterol, 1 CG mini-B, 1 CG SP-C molecules and some water and Na^+ beads was built. The system is minimized for 2000 steps, then heated to 293 K, followed by an NPT equilibration at π= 30 mN/m in which only the system dimensions parallel to the GO membrane were allowed to change. Then this system was equilibrated in the NVT ensemble. This equilibrated small system was tiled to 6×6 times in the x-y plane and redundant protein molecules were removed. An NVT equilibration as long as 1 ms was executed on this large system and the last frame was extracted and used for following simulations.

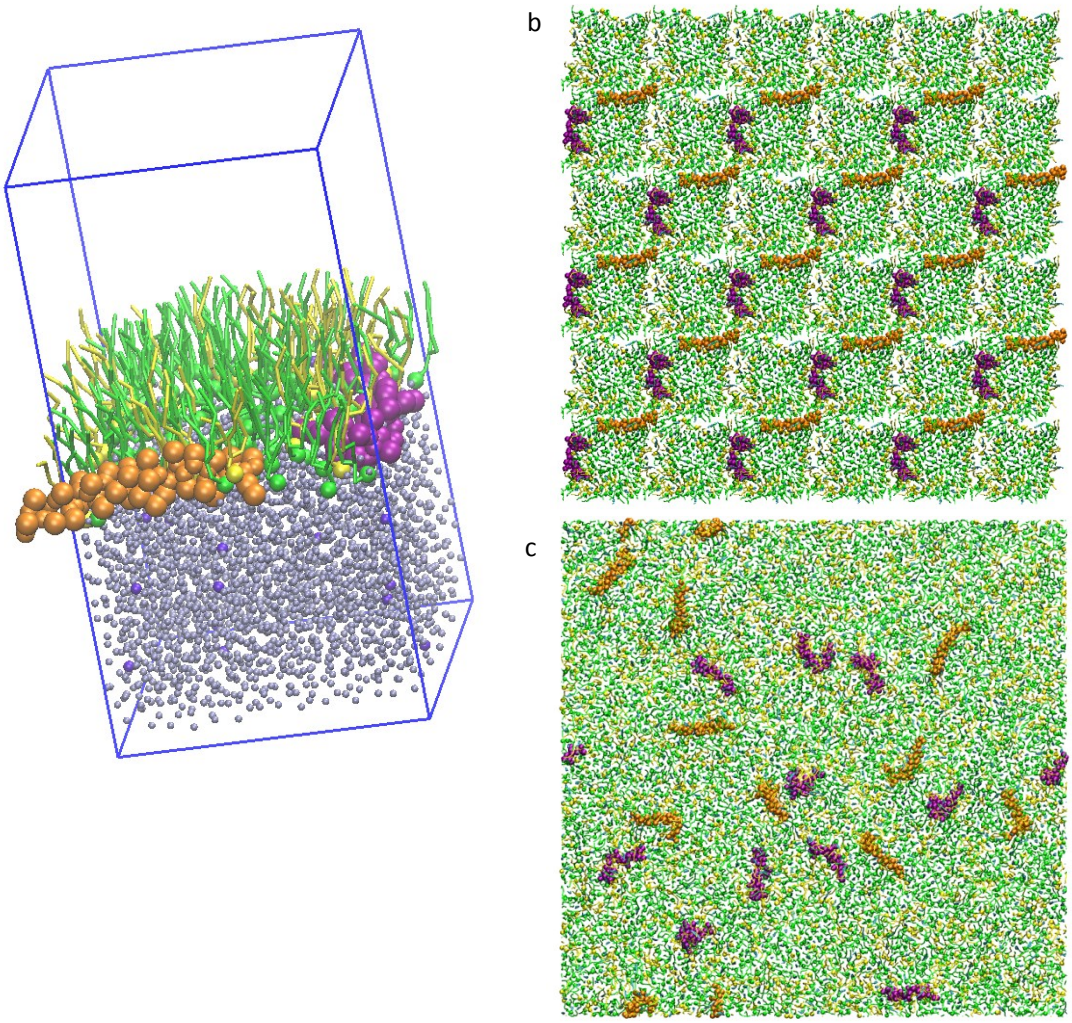

Figure S2. Obtaining a stable PS monolayer interface. (a) The stable state of the small system, the blue box is for the periodic boundaries. (b) This small system was tiled to 6×6 times in the x-y plane and redundant protein molecules were removed. (c) The stable large system. Color scheme: DPPC in green, POPG in yellow, cholesterol in cyan, SP-C in orange, mini-B in purple, water in ice blue, ions in violet. Water and ions are only shown in (a) for clarity.

The effect of orientations of GO when interacting with the PS monolayer. As the GO nanosheet is a 2D nanomaterial, the orientation in which they contact with the PS monolayer from the air side may affect the result of the interaction. In fact, Li et al showed that the edges and corner of graphene nanosheet play an important role in interaction with lipid bilayer.[14] To study the effect of the orientations, systems with GO nanosheets in three different initial orientations are simulated. As the nanosheets move randomly before it contacts the monolayer, different initial orientations mean different randomly orientations when contact. All orientations lead to similar results as shown in Figure S3. These indicate that the orientation of GO nanosheets rarely influences the GO-PS interaction.

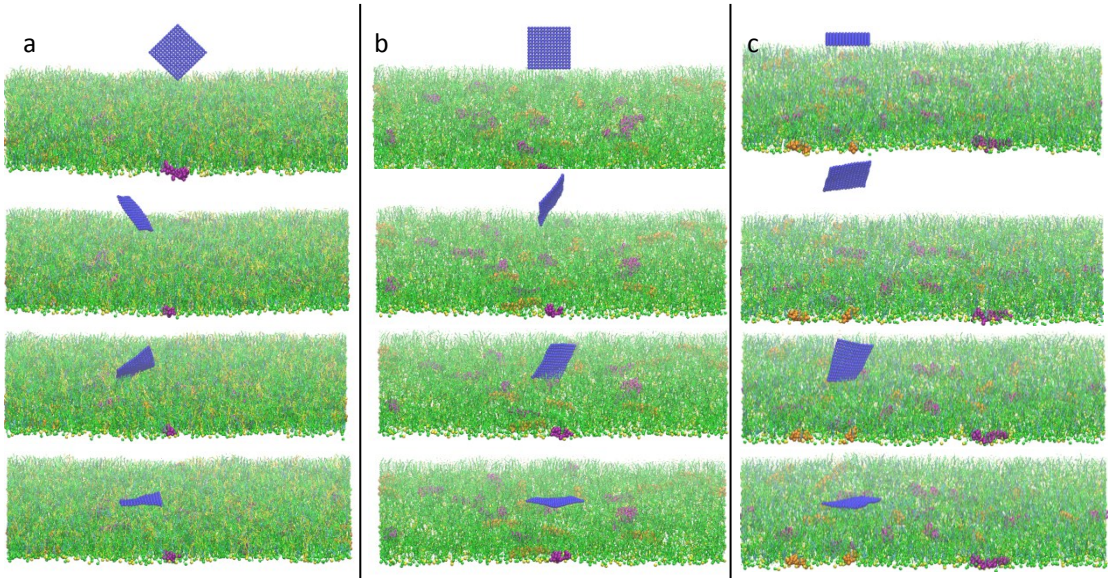

Figure S3. Simulations on the effect of orientations of GO. GO with three different initial orientations are simulated. (a-c) shows processes of the three different orientations, to show the change of the GO orientation clearly, a side view with tilted 15 degree is chosen. As the orientation changes irregularly, the GO touch the PS with a random orientation, but the GO nanosheet finally lies down on the PS monolayer regardless of its initial orientation. Color scheme: DPPC in green, POPG in yellow, cholesterol in cyan, SP-C in orange, mini-B in purple, graphene oxide in blue. Water and ions are not shown for clarity.

Calculation of order parameter. The order parameter was calculated for each bead of DPPC, POPG, and cholesterol molecules except the first and last ones of each chain, using the equation

$$S_z = \frac{3}{2}\cos^2\theta_z - \frac{1}{2},$$

varying from -0.5 to 1. The θ_z is the angles between the z-axis and the vector connecting the two adjacent beads C_{n-1}, C_{n+1}.[15] (i.e. for the POPG molecule shown in Figure S4, pairs GL1-C2A, C1A-C3A,and C2A-C4A are used for calculated order parameters of C1A, C2A, and C3A respectively.) The Voronoi diagram was determined by the centers of all beads of lipid tails, and colored by the averaged order parameter of the chain. (i.e. for POPG molecule shown in Figure S4, position of the right chain is determined by the center of beads GL1, C1A, C2A, C3A, and C4A, and order parameter is determined by those of C1A, C2A, and C3A.)

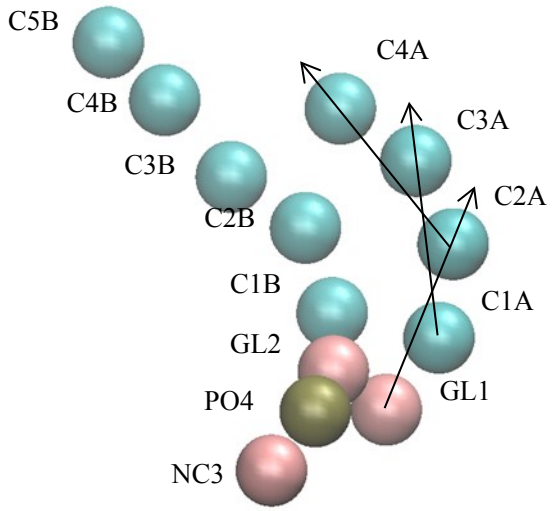

Figure S4. CG model of a POPG molecule used as an example to explain the calculation of the order parameter.

Interaction between GO and surfactant proteins. In our previous study,[7] we also found that surface charge of NPs regulates their affinity to surfactant proteins and the anionic NPs may adsorb SP-B. In this work, no obvious attraction or repulsion is found between the proteins and the electrically neutral GO nanosheet. SP-B and SP-C may stay under the GO nanosheet, only depending on whether the GO nanosheet contacts a protein-containing area. For 10×10 nm^2 monolayer GO nanosheet, the averaged GO-proteins and GO-lipids VdW energy are -88 and -3411 kJ/mol, respectively. As the contact area between GO and lipids is a few dozen times larger than that between GO and proteins, these data indicate no significant difference between these two types of interactions.

The radial distribution function. The radial distribution function (RDF) (also known as pair correlation function g(r)) describes how density of particle varies with distance from a reference particle. By showing the correlation between components, it can be used to reflect the phase behaviors and homogeneity of lipid membranes. In-plane RDFs between lipid heads are shown in Figure S5. Using A, B to represent two kinds of lipid heads (NC3 beads in DPPC, GL0 beads in POPG, and ROH beads in cholesterol) specified by four associations (DPPC-DPPC, POPG-POPG, DPPC-POPG, and cholesterol-cholesterol), the RDFs between A and B are calculated following the equation

$$g_{AB}(\mathrm{r}) = \frac{<\rho_B(r)>}{\rho_B},$$

with $<\rho_B(r)>$ the averaged density of B at a distance r around A, and $<\rho_B>$ the density of type B averaged over all the system. It can be found that the monolayer GO nanosheets hardly impact the RDFs, but the trilayer nanosheets finitely perturb the RDFs for phospholipids (Figure S6). This difference is believed to come from the stronger VdW interactions between the trilayer GO nanosheet and the PS molecules.

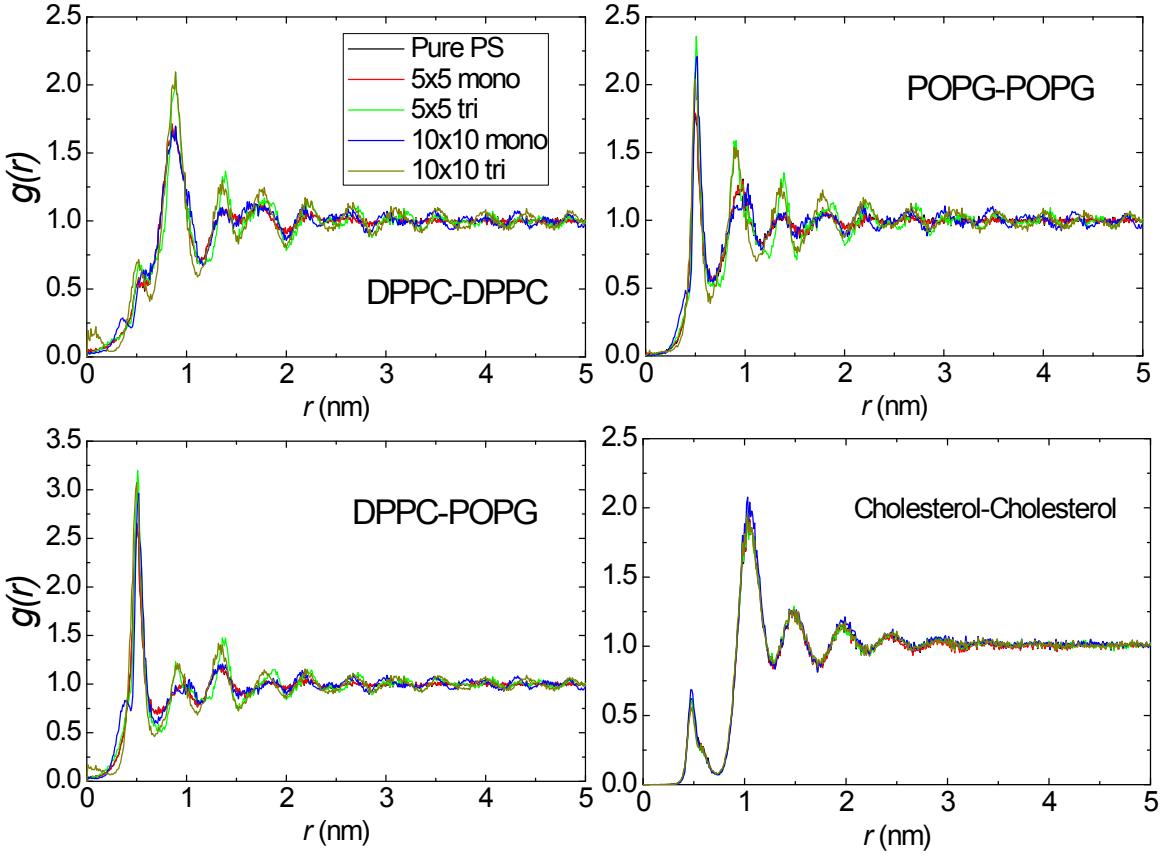

Figure S5. Impact of GO on the In-plane radial distribution function (RDF) of PS. For pure PS and PS affected by GO of all the four types (5×5 nm^2 monolayer, 5×5 nm^2 trilayer, 10×10 nm^2 monolayer, 10×10 nm^2 trilayer), the RDFs for DPPC-DPPC (a), POPG-POPG (b), DPPC-POPG (c), cholesterol-cholesterol (d) association are plotted. In general, GO nanosheets hardly impact the RDFs, although trilayer nanosheets finitely perturb the RDFs for phospholipids.

Interaction between the PS monolayer and reduced-GO and graphene. Interaction between GO with half of the oxide function groups reduced and PS is simulated. The reduced-GO was built by randomly changing half of the beads (SN0 and SP2) in the 5×5 nm^2 monolayer GO nanosheet to graphene beads (SC4). No pore appears on the PS and the order parameter and diffusion coefficients are much more similar to those of a pure PS rather than those of a GO-affected PS (Figure S6). We believe that it is the pores not the GO itself affect the monolayer properties directly.

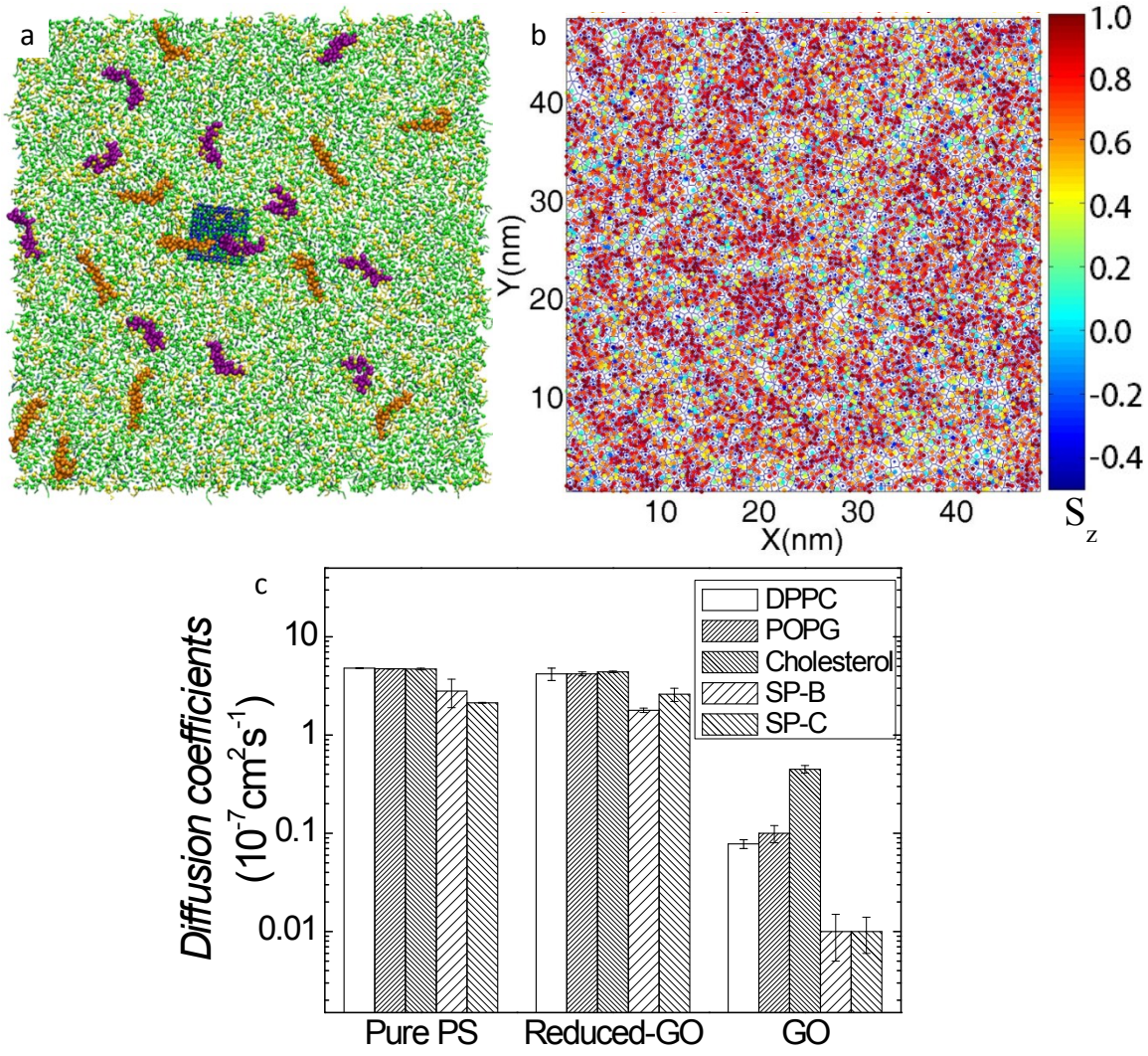

Figure S6. Impact of reduced GO on the PS. Reduced-GO with half oxide groups stays on the monolayer without pore induced (a). Order parameter (b) and diffusion coefficients (c) of reduced-GO-affected PS monolayer are much more similar to those of a pure PS rather than those of a GO-affected PS. We believe that it is the pores not the GO itself affect the monolayer properties directly.

Experimental materials and methods.

Pulmonary Surfactant. Infasurf (calfactant) is a modified natural surfactant prepared from lung lavage of newborn calves by centrifugation and organic solvent extraction. Infasurf contains all hydrophobic components of the bovine natural surfactant.[16] Hydrophilic surfactant protein was removed during the extraction process. Infasurf was stored frozen in sterilized vials with an initial concentration of 35 mg total phospholipids per milliliter. Before experiment it was diluted to 5mg/mL by a saline buffer of 0.9% NaCl, 1.5 mM $CaCl_2$, and 2.5 mM HEPES, adjusted to pH 7.0.

Langmuir-Blodgett Trough. Spread, compression, and Langmuir-Blodgett (LB) transfer of surfactant films were conducted with a LB trough (KSV Nima, Coventry, UK) at room temperature (20 ± 1 ℃). A detailed experimental protocol can be found elsewhere.[17-20] Before the experiment, GO nanosheets were mixed and co-spread with 5 mg/mL Infasurf to a concentration of 50 μg/mL, namely, the mixing ratio between GO and Infasurf was 1:100. The co-spread films were compressed at a rate of 20 cm^2/min (0.1% initial surface area per second), until the demanded surface pressure is reached. For AFM imaging, Infasurf films at the air-water interface were transferred to the surface of freshly cleaved mica using the LB technique. Surfactant films at controlled constant surface pressure were deposited onto the mica surface by elevating the previously submerged mica vertically through the air-water interface at a rate of 1 mm/min. Deposited films were scanned by AFM within 2 h of deposition. The nanostructure of the PS monolayer affected by GO are obtained by AFM, along with that without GO at the same surface pressure as a control.

Constrained Drop Surfactometer. Biophysical properties of pure Infasurf and Infasurf affected by GO were tested using a constrained drop surfactometer (CDS). The CDS is a droplet-based surface tensiometer.[18,19] By periodically changing the droplet volume, the CDS can get the relationship between the area and surface tension of lung surfactant at a physiologically relevant cycling rate, thus assess its biophysical properties.[21] The concentration GO was set to 10 μg/mL, and the Infasurf concentration was 1 mg/mL, to keep the weight ratio 1:100. About 10 μL of the GO−Infasurf mixture was dispensed onto the CDS drop pedestal. After the droplet formatted and reached equilibrium, the droplet was compressed and expanded at a rate of 3 s per cycle with a controlled compression ratio less than 50% to simulate normal tidal breathing. Continuous compression−expansion cycles were executed for each droplet until the cycles became repeatable. More details can be found in our previous papers.[18,19]

Experimental result at different surface pressures. We have tested the PS-GO interaction at different surface pressures. Lateral structures of PS films with exposure to GO at four characteristic surface pressures (π) of 20, 30, 40, and 50 mN/m are obtained using the same method described in the text (Figure S7). It can be found that GO deposits at the PS at all these four surface pressures.

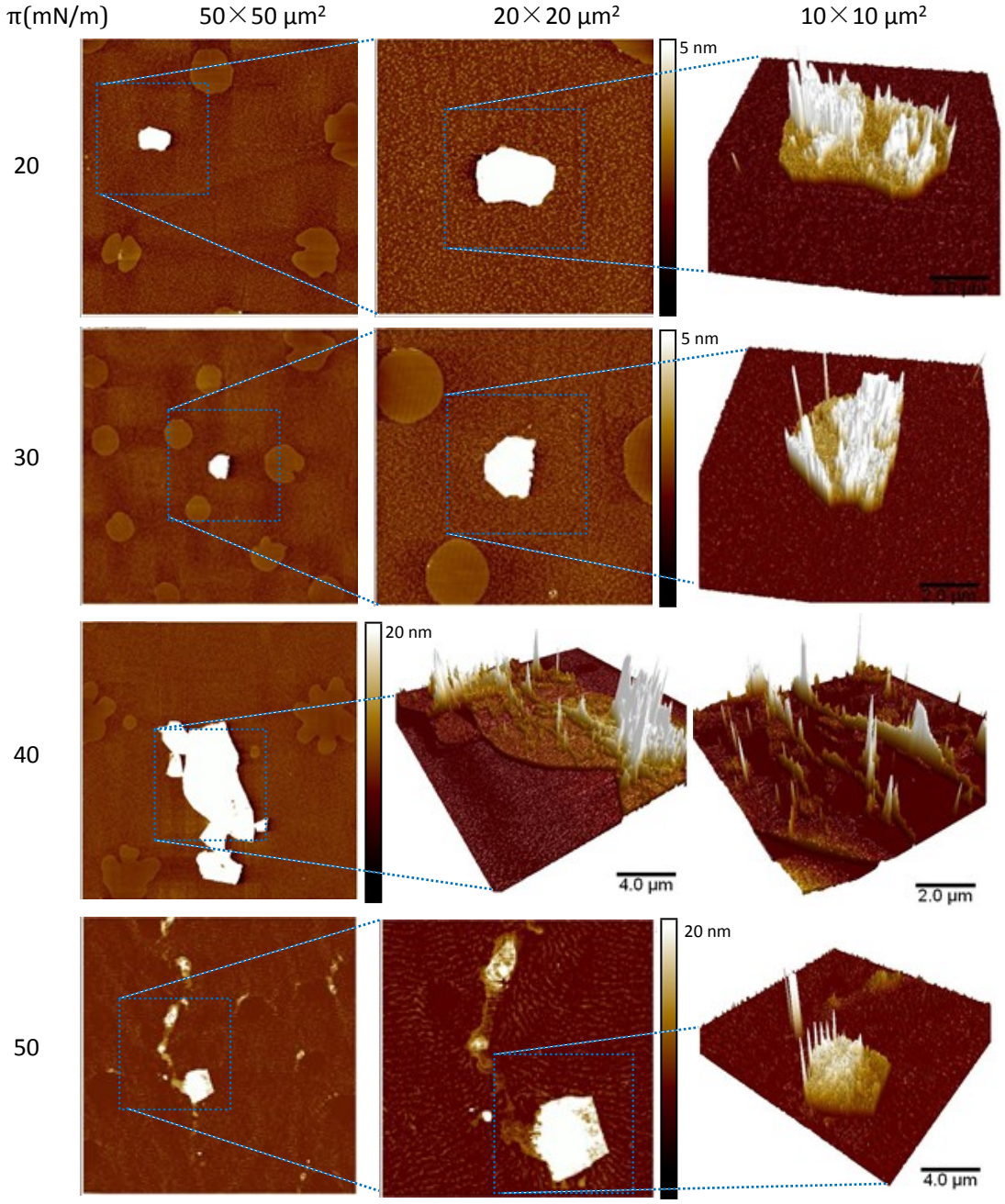

Figure S7. Nanostructure of the PS monolayer affected by GO at different surface pressures. For PS films with exposure to GO at four characteristic surface pressures (π) of 20, 30, 40, and 50 mN/m, lateral structures of different scan areas of 50×50, 20×20, and 10×10 μm² are shown. 3D images show the lipids on the GO nanosheet.

References

1 S. J. Marrink, H. J. Risselada, S. Yefimov, D. P. Tieleman, A. H. de Vries, *J. Phys. Chem. B* 2007, **111**, 7812.

2 A. Lerf, H. Y. He, M. Forster, J. Klinowski, *J. Phys. Chem. B* 1998, **102**, 4477.

3 D. Wu, X. Yang, *J. Phys. Chem. B* 2012, **116**, 12048.

4 A. Bagri, C. Mattevi, M. Acik, Y. J. Chabal, M. Chhowalla, V. B. Shenoy, *Nat. Chem.* 2010, **2**, 581.

5 P. Johari, V. B. Shenoy, *ACS Nano* 2011, **5**, 7640.

6 E. Keating, Y. Y. Zuo, S. M. Tadayyon, N. O. Petersen, F. Possmayer, R. A. Veldhuizen, *Biochim. Biophys. Acta* 2012, **1818**, 1225.

7 G. Hu, B. Jiao, X. Shi, R. P. Valle, Q. Fan, Y. Y. Zuo, *ACS Nano* 2013, **7**, 10525.

8 S. Baoukina, E. Mendez-Villuendas, D. P. Tieleman, *J. Am. Chem. Soc.* 2012, **134**, 17543.

9 F. Baumgart, O. L. Ospina, I. Mingarro, I. Rodriguez-Crespo, J. Perez-Gil, Biophys. J. 2010, **99**, 3234-3243.

10 B. Hess, C. Kutzner, D. van der Spoel, E. Lindahl, *J. Chem. Theory Comput.* 2008, **4**, 435.

11 L. M. Gordon, K. Y. C. Lee, M. M. Lipp, J. A. Zasadzinski, F. J. Walther, M. A. Sherman, A. J. Waring, *J. Pept. Res.* 2000, **55**, 330.

12 M. Sarker, A. J. Waring, F. J. Walther, K. M. Keough, V. Booth, *Biochemistry* 2007, **46**, 11047.

13 A. J. Waring, F. J. Walther, L. M. Gordon, J. M. Hernandez-Juviel, T. Hong, M. A. Sherman, C. Alonso, T. Alig, A. Braun, D. Bacon, J. A. Zasadzinski, *J. Pept. Res.* 2005, **66**, 364.

14 Y. Li, H. Yuan, A. von dem Bussche, M. Creighton, R. H. Hurt, A. B. Kane, H. Gao, *Proc. Natl. Acad. Sci. U. S. A.* 2013, **110**, 12295.

15 X. Lin, Y. Li, N. Gu, *Soft Matter* 2011, **7**, 3882.

16 M. S. Bakshi, L. Zhao, R. Smith, F. Possmayer, N. O. Petersen, *Biophys. J.* 2008, **94**, 855.

17 Q. Fan, Y. E. Wang, X. Zhao, J. S. Loo, Y. Y. Zuo, *ACS Nano* 2011, ***5***, 6410.

18 R. P. Valle, T. Wu, Y. Y. Zuo, *ACS Nano* 2015, **9**, 5413.

19 R. P. Valle, C. L. Huang, J. S. C. Loo, Y. Y. Zuo, *ACS Sustainable Chem. Eng.* 2014, **2**, 1574.

20 H. Zhang, Q. Fan, Y. E. Wang, C. R. Neal, Y. Y. Zuo, *Biochim. Biophys. Acta* 2011, **1808**, 1832.

21 L. M. Yu, J. J. Lu, Y. W. Chan, A. Ng, L. Zhang, M. Hoorfar, Z. Policova, K. Grundke, A. W. Neumann, *J. Appl. Physiol.* 2004, **97**, 704.